Journal of Water Resource and Protection, 2026, 18(11), 836-853
https://www.scirp.org/journal/jwarp
ISSN Online: 1945-3108
ISSN Print: 1945-3094

Assessing Mine Dewatering Discharges through Coupled UAV Imagery and 1D Hydraulic Modeling: A Case Study at Bonikro Gold Mine, Southwestern Côte d'Ivoire

Blaise Koffi Yao[1*], Mamadou Touré[1], Kamagaté Anzoumanan[2], Derving Baka[1]

[1]Laboratory of Soil, Water and Geomaterials Sciences, Training and Research Unit in Earth Sciences and Mining Resources, University Félix Houphouët-Boigny, Abidjan, Côte d'Ivoire
[2]Polytechnic University of San-Pedro, San-Pedro, Côte d'Ivoire
Email: *yaomonie@yahoo.fr

How to cite this paper: Yao, B.K., Touré, M., Anzoumanan, K. and Baka, D. (2026) Assessing Mine Dewatering Discharges through Coupled UAV Imagery and 1D Hydraulic Modeling: A Case Study at Bonikro Gold Mine, Southwestern Côte d'Ivoire. *Journal of Water Resource and Protection*, **18**, 836-853.
https://doi.org/10.4236/jwarp.2026.1811041

Received: September 1, 2026
Accepted: November 17, 2026
Published: November 20, 2026

Copyright © 2026 by author(s) and Scientific Research Publishing Inc.
This work is licensed under the Creative Commons Attribution International License (CC BY 4.0).
http://creativecommons.org/licenses/by/4.0/
Open Access

Abstract

The management of mine dewatering effluents is one of the major environmental challenges of open-pit mining. This study, commissioned by the Bonikro Gold mine (Côte d'Ivoire), assesses the hydraulic impact of discharging pit dewatering waters—estimated at about 3,000,000 m^3—into the downstream alluvial floodplain. The methodology integrates drone-based mapping (DJI Phantom 4 RTK), total-station topographic surveys, hydrogeomorphological identification of stream channels, and one-dimensional hydraulic modeling with HEC-RAS over 29 cross-sections spanning about 8 km. Four pumping-flow scenarios were simulated: no pumping (baseline), 200 m^3/h, 400 m^3/h and 600 m^3/h. The results show that the baseline condition produces a flooded area of 16.9 ha, whereas the 200, 400 and 600 m^3/h scenarios generate 116.2 ha, 53 ha and 158 ha, respectively. The 400 m^3/h scenario appears the most favorable: at this flow, the minor and intermediate channels can contain the discharge without excessive overflow. Field validation of the 600 m^3/h scenario corrected the modeled estimate (158 ha) to 99.57 ha of actually flooded area. These results support operational recommendations for minimizing impacts on riparian agricultural land and illustrate the value of combining UAV technologies with HEC-RAS modeling for environmental decision support in the African mining sector. The 400 m^3/h scenario should nevertheless be regarded as a conditional optimum, valid only for the pumping duration and the season under which it was established (dry-season, low-flow conditions). The

field-validated area of 99.57 ha is a proxy derived from flood-indicator vegetation and field water marks.

Keywords

Mine Dewatering, HEC-RAS, Flood Hazard Mapping, UAV Photogrammetry, Côte d'Ivoire

1. Introduction

Against a backdrop of recent climate change that is increasing the frequency and intensity of rainfall events in West Africa, river floods regularly affect agricultural areas and represent a growing threat to the livelihoods of rural communities [1]. In this context of vulnerability, the gold-mining sector, which has grown considerably in sub-Saharan Africa and particularly in Côte d'Ivoire since the 2000s [2], adds additional pressure on ecosystems. Indeed, open-pit mining generates considerable volumes of groundwater and surface water that can accumulate in extraction pits. These waters, known as mine dewatering, must be evacuated to allow mining operations to continue. Their discharge into adjacent receiving hydrosystems constitutes a potentially severe hydrological and hydraulic disturbance, especially in humid tropical zones with dense hydrographic networks and heavily anthropized alluvial plains [3]. Proactive management of these mine discharges is therefore essential.

The Bonikro Gold mine, located in the Centre-West region of Côte d'Ivoire, is one of the most important gold operations in the sub-region. Draining its main pit, which holds about 3,000,000 m^3 of water, forces the release of massive hydraulic volumes into the downstream alluvial plain, an area used by local populations for cash and food crops. Although flood problems induced by anthropogenic activities are increasingly documented worldwide [4] [5], their local assessment requires precise tools. Coupled hydraulic modeling and remote-sensing mapping have emerged as essential approaches [6] [7]. The HEC-RAS (Hydrologic Engineering Center-River Analysis System) model, developed by the US Army Corps of Engineers (USACE), is widely used for simulating open-channel flow and delineating flood-prone areas [8] [9]. However, the accuracy of these models depends heavily on the resolution of the input topographic data. In this respect, low-altitude aerial drone photogrammetry represents a major technological advance: drones equipped with RTK (Real-Time Kinematic) systems achieve centimeter-level accuracy at reduced cost, even in inaccessible areas [10]-[12]. This synergy between hydraulic models and drone imagery provides a unique opportunity to reduce uncertainty in flood-risk delineation [13] [14].

Within this framework, the present study aims to: i) establish the current water extent in the riparian agricultural plots; ii) map the stream beds and preferential flood-prone areas; iii) model the hydraulic impact of different dewatering dis-

charge scenarios on the downstream flood extent; and iv) formulate operational recommendations for managing the discharge of Bonikro Gold pit dewatering waters.

2. Materials and Methods

2.1. Study Area

The Bonikro Gold mine is located in the Lôh-Djiboua region, in the Centre-West of Côte d'Ivoire, in the department of Oumé. The mining site lies near the locality of Hiré, between the towns of Oumé and Divo. The study area covers the alluvial plain downstream of the dewatering outfall, over a length of about 8 km and a variable width of about 600 m (Figure 1).

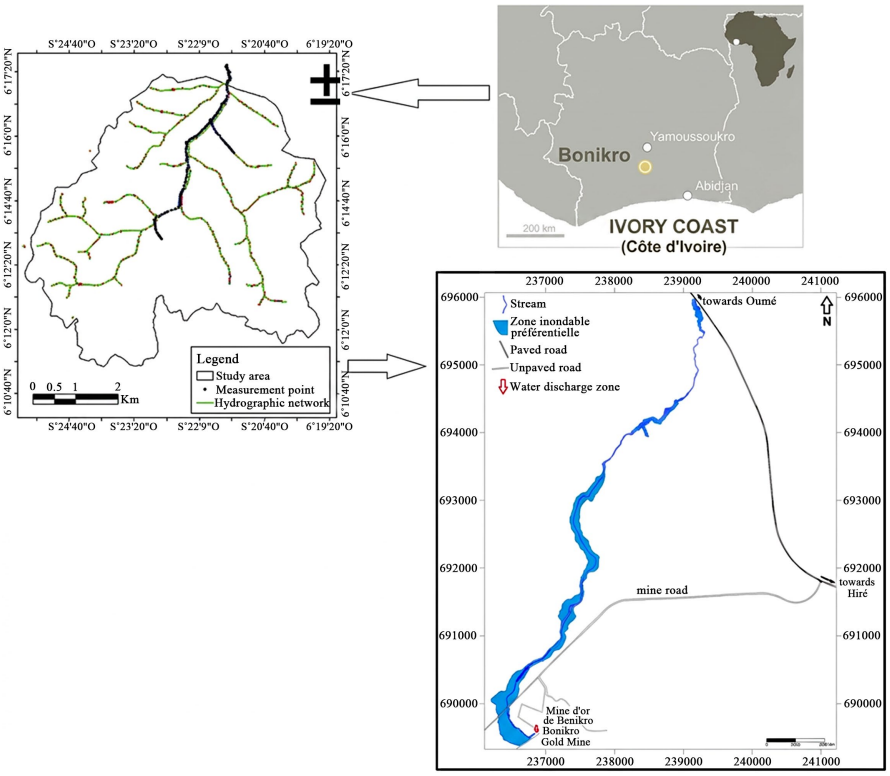


Figure 1. Location of the study area.

The region is characterized by a gently undulating plateau typical of the Precambrian basement of West Africa. The streams show a pronounced meandering character with numerous lowlands and marshy zones that constitute potentially flood-prone areas. The hydrological regime is tropical with two rainy seasons (long rainy season: March-July; short rainy season: September-November) and two dry seasons (long dry season: November-March; short dry season: August). The alluvial plain downstream of the mining site is densely occupied by farmers practicing market gardening (in the dry season, in the humid lowlands) and food cropping (in the rainy season). The presence of these riparian farms makes the area highly vulnerable to the anthropogenic floods induced by the discharge of

dewatering waters.

Precipitation is substantial and can exceed 350 mm/month during the long rainy season (Figure 2).

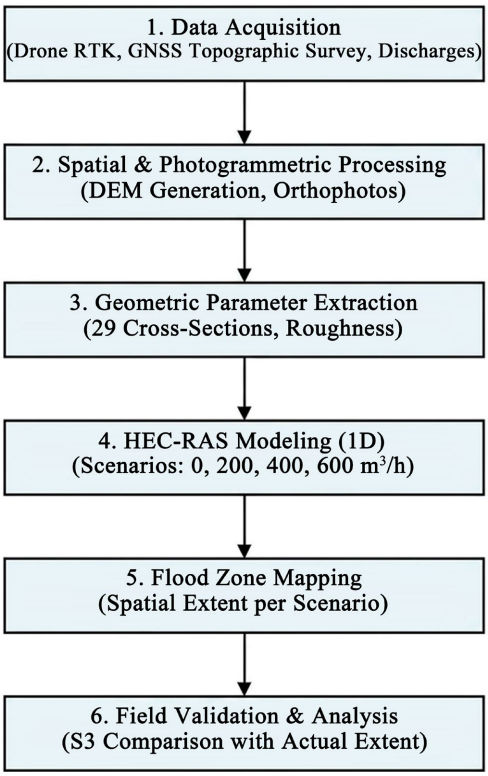


Figure 2. Methodological flowchart of the study.

2.2. Materials and Data

To carry out the hydrological risk assessment and flood modeling, a variety of equipment and data were mobilized. Field data acquisition relied on piezometric probes, topographic survey equipment (differential GPS, D-RTK2 base), drones (Phantom 4 RTK) for high-resolution photogrammetry, and standard measuring equipment (tape measures, cameras). The data exploited include historical rainfall series (provided by SODEXAM), 30-m SRTM digital elevation models, geological maps at 1/500,000, and satellite images (Sentinel-2). The data used by the HEC-RAS model comprise: i) geometric data—29 cross-sections measured in the field and described by distance-elevation pairs, Manning roughness coefficients (n) determined according to the nature of the bed and riparian vegetation, distances between successive sections (banks and channel axis), and contraction/expansion coefficients; and ii) hydraulic data and boundary conditions—the simulated flows (Q_natural (no-pumping state), Q1 = 200 m^3/h (55.6 l/s), Q2 = 400 m^3/h (111.1 l/s), Q3 = 600 m^3/h (166.7 l/s)), an upstream boundary condition (imposed flow) and a downstream condition (normal depth calculated from the bed slope). ArcGIS 10.4 and HEC-RAS were respectively used for spatial processing and hydraulic modeling. The three pumping discharges simulated (200, 400 and 600

m^3/h) are superimposed on the natural upstream discharge of the receiving watercourse; they do not replace it. The natural reference discharge corresponding to the no-pumping state (scenario S0) is Q_natural (138.96 m^3/h (38.6 l/s)), estimated from field gauging at the study reach during the field campaign. Scenarios S1, S2 and S3 therefore correspond to Q_natural + 200, Q_natural + 400 and Q_natural + 600 m^3/h respectively.

Three roughness zones were parameterized, corresponding to the three bed levels identified in the field: i) the minor bed (active channel), ii) the intermediate bed (seasonally flooded and partly cultivated), and iii) the major bed (floodplain). The Manning coefficient n retained for each zone, the surface it represents and the basis of its selection are given in Table 1. The values were first assigned from the land-use classification derived from the drone orthophotographs and were then constrained by calibration against the observed water levels and the flood marks recorded during the field campaign, within the roughness ranges recommended in the HEC-RAS Hydraulic Reference Manual [8]. Roughness was assigned from the land-use classification derived from the drone orthophotographs.

Table 1. Manning roughness coefficients retained for each bed level.

Roughness zone	Manning n	Surface/vegetation	Selection basis
Minor bed (active channel)	0.035	bare bed, sand-gravel, sparse aquatic plants	field observation + calibration; within the HEC-RAS manual range [8]
Intermediate bed	0.050	dry-season market gardening, herbaceous and crop cover	land-use classification from drone orthophoto
Major bed (floodplain)	0.080	dense hygrophilous vegetation, crops and trees	land-use classification; not represented in the computed conveyance

2.3. Methods

To identify and map the flood extent in the downstream plain of Bonikro as a function of rainfall and pit pumping flows, a multi-source approach was adopted (drone remote sensing, GPS/GNSS topographic surveys and hydraulic modeling). This combination is justified by the complementarity of the data. Drone imagery provided fine spatial coverage for mapping land use, locating lowlands/marshes and determining the geometry of the plain and the channel, as recognized in many flood-hazard mapping studies based on UAV/photogrammetry platforms [15] [16]. Topographic surveys and GNSS/GPS coordinates served to calibrate and verify the positions and elevations used in the processing chain and in the hydraulic model, an essential step to limit georeferencing errors and ensure the consistency of profiles/sections. The hydraulic assessment of the water extent was performed with HEC-RAS, integrating the morphology, the cross-sections and flow scenarios related to rainfall and pumping [17].

The 1D HEC-RAS model relies on the resolution of the Saint-Venant equations for one-dimensional flow. These equations, formulated by Saint-Venant in 1871, describe the quasi-one-dimensional flow in a channel or watercourse of width $l(x)$.

The cross-sectional area of the flow is $A(x, t)$ and the mean flow velocity is $U(x, t)$. The water depth is $h(y, t)$, measured from the bed $z = 0$. The mass-conservation equation is written as:

$$\frac{\partial A}{\partial t} + \frac{\partial (AU)}{\partial x} = 0 \tag{1}$$

The longitudinal momentum equation is written as:

$$\frac{\partial (hU)}{\partial t} + \frac{\partial (hU^2)}{\partial x} + gh\frac{\partial h}{\partial x} = \frac{\tau x}{\rho} \tag{2}$$

where $\tau x(X, t)$ is the shear applied to the wetted perimeter $P(x, t)$.

The equation in Z is given by the hydrostatic equilibrium:

$$\frac{\partial p}{\partial z} = \rho g \tag{3}$$

This approach required precise parameterization of the Manning roughness coefficient, calibrated here from the detailed land-use classification derived from drone orthophotographs.

The model results were then validated by direct comparison with flood marks observed in situ. The global logic of the method is therefore to: i) produce a reliable and contextualized spatial base (drone + recognition of vulnerable zones); ii) consolidate the geometry with field measurements (GPS/GNSS); iii) transform this information into water-extent maps under scenarios; and iv) reinforce the results with field validation elements (comparison and check of the actually flooded zones). Four discharge scenarios were therefore defined: i) Scenario S0—no pumping (natural reference state); ii) Scenario S1—pumping flow of 200 m^3/h; iii) Scenario S2—pumping flow of 400 m^3/h; and iv) Scenario S3—pumping flow of 600 m^3/h. Model validation was carried out for the most critical scenario S3 (600 m^3/h). A complementary field mission compared the flooded areas predicted by the model with the actually flooded areas, combining modeling, topographic and hygrophilous vegetation analysis data as an indicator of the real flood extent. The Gravelius compactness index is given by:

$$Kc = 0.282\frac{p}{\sqrt{A}} \tag{4}$$

where P is the watershed perimeter (km) and A the watershed area (km^2).

The hydraulic simulations were performed with HEC-RAS version [5.0.x] using a one-dimensional steady-state (permanent, gradually varied flow) run type, in a subcritical flow regime, solved by the standard-step method. The computational domain comprises 29 cross-sections spaced on average 3 m apart over a reach of about 8 km, with contraction and expansion coefficients of 0.1 and 0.3 respectively. The upstream boundary condition is a prescribed total discharge (the scenario flow, equal to Q_natural plus the pumping discharge); the downstream boundary condition is normal depth with a friction slope equal to the mean bed slope of the reach (0.08m/m). Rainfall is excluded from the simulations: no rainfall-runoff input is imposed, the model describing solely the hydraulic response

of the channel to the imposed discharge under dry-season conditions. The total volume of dewatering water considered is about 3,000,000 m^3; pumped at 400 m^3/h, this corresponds to a continuous pumping schedule of about 7500 h (312 days). Each scenario was run to convergence of the water-surface profile. The hydrographs are not required in this steady-state framework; the single discharge of each scenario replaces a time-varying inflow, and the pumping volume is accounted for through the duration of the schedule rather than through a routed hydrograph.

The 600 m^3/h scenario (S3) was validated during the dry-season field campaign of January-February 2021. The validation protocol comprised: i) GNSS/D-RTK2 georeferenced mapping of the actually flooded and waterlogged zones; ii) recording of flood marks and of the limits of standing water; iii) survey of the discharge actually pumped at the outfall and of the effective pumping schedule at the time of the observations; and iv) mapping of hygrophilous (flood-indicator) vegetation and of residual soil moisture used as an indicator of the maximum recent flood extent. The validated flooded area of 99.57 ha is therefore a proxy: it is derived from the flood-indicator vegetation, the residual soil moisture and the field water marks, rather than from a synoptic measurement of the water surface. It is representative of the maximum dry-season flood extent under the documented discharge and must not be read as a synchronized hydraulic measurement.

3. Results

3.1. Morphological and Hydrographic Characteristics of the Study Area

Drone mapping and topographic surveys revealed a strongly meandering fluvial morphology, characteristic of lowland watercourses in tropical environments. The stream is highly sinuous with a high sinuosity index. Numerous lowlands and marshy zones were identified along the watercourse, constituting potentially flood-prone areas. The hydrogeomorphological analysis distinguished three bed levels: i) the minor bed (active channel), a permanent, well-defined channel of variable width; ii) the intermediate bed, flooded during frequent floods and partly occupied by market gardens in the dry season; and iii) the major bed, representing the maximum flood extent and including the most exposed riparian plantations. During the field mission (dry season, February 2021), the only flooded areas observed corresponded to the humid lowlands of the intermediate bed. Testimonies from local farmers confirmed that the stream regularly overflowed its banks in the rainy season, flooding adjacent plantations.

The morphometric characteristics of the study sub-watershed are: a perimeter of 46 km, an area of 86 km^2, a main watercourse length of 11 km, and a Gravelius coefficient of 1.38. This coefficient, defined as the ratio of the studied basin perimeter to that of a circle of equal area, allows the basin shape to be evaluated [18]. A value of 1 characterizes a perfectly circular basin; the value of 1.38, significantly above 1, indicates that the studied sub-basin has a clearly elongated shape [19].

From a hydrodynamic point of view, this elongated morphology exerts a major control on the genesis and propagation of flows: it induces a longer concentration time than a circular basin of equal area [20]. The path of the water over the 11-km main course delays the arrival of flows from the most distant points of the basin, so that the runoff volumes do not converge simultaneously at the outlet. This temporal lag is reflected on the hydrograph as a spread of the flood over time and a natural attenuation of the flood peak [21]. Unlike a circular (fan-shaped) basin prone to sudden, violent floods, this elongated geometry provides relative regulation of peak flows.

Drone mapping made it possible to locate and delimit precisely the agricultural plots located in the intermediate and major beds. These plots are mainly used for market gardening (tomatoes, eggplants, peppers, okra) in the dry season, taking advantage of the residual moisture of the lowlands, and for food crops (cassava, maize, yam) in the rainy season on the higher parts (**Figure 3**).

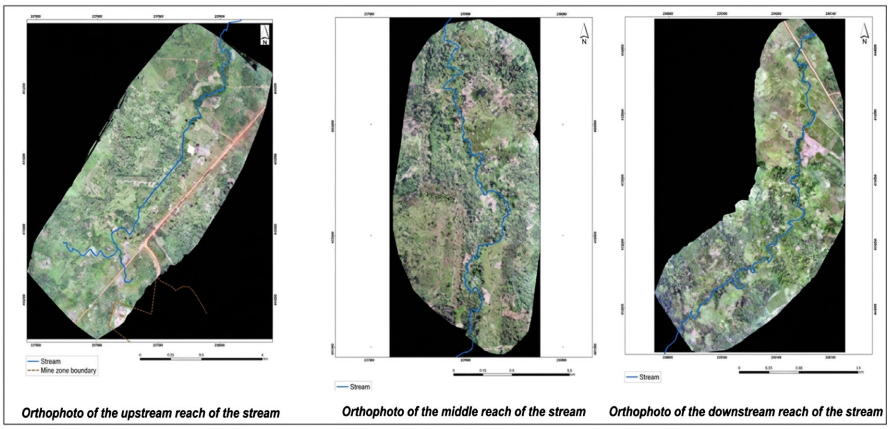


Figure 3. Orthophoto of the upstream part of the watercourse.

3.2. Hydraulic Modeling Results

The HEC-RAS simulations provided, for each scenario, the mapping of the flooded zones and the corresponding areas, presented in **Table 2**. The corresponding hydraulic diagnostic variables (water-surface elevation, velocity and conveyance) are presented in **Table 3** and analysed below.

Table 2. Flooded areas according to the pumping-flow scenarios.

Scenario	Flow (m^3/h)	Flooded area (ha)	Observation
S0 (no pumping)	0	16.9	Natural reference state
S1 (low pumping)	200	116.2	Stagnation and lateral overflow
S2 (optimal pumping)	400	53.0	Channelized flow in the beds
S3 (high pumping)	600	158.0 (model)/99.57 (field)	Overflow of the beds

The results show a non-monotonic relationship between the discharge and the

flooded area, with a minimum flood obtained for scenario S2 (400 m^3/h). This atypical relationship is explained by the following hydraulic mechanisms: i) Scenario S1 (200 m^3/h): the discharge is insufficient to induce an effective flow in the channel, favoring water stagnation in the lowlands and meanders and generating extensive lateral overflow zones (116.2 ha) [22]; ii) Scenario S2 (400 m^3/h): this flow corresponds to the optimal hydraulic capacity of the combined minor and intermediate beds; the kinetic energy of the flow is sufficient for the water to flow efficiently in the channel without excessive overflow, limiting the flooded area to 53 ha; iii) Scenario S3 (600 m^3/h): the discharge exceeds the transport capacity of the minor and intermediate beds, causing generalized overflow into the major bed. The modeled flooded area is 158 ha, corrected to 99.57 ha after field validation. The 58.43 ha gap (58.7% relative to the field-validated area of 99.57 ha) between the model and the field reflects the inherent limitations of 1D modeling, in particular the non-consideration of vegetation roughness in the major bed and of anthropogenic obstacles. Correction of the relative error: the value of 37% reported in the earlier version was obtained by using the modelled area (158 ha) as denominator. The correct reference for quantifying the overestimation of the model is the field-validated area (99.57 ha), which gives 58.7%.

Table 3. Hydraulic diagnostic variables for each pumping-flow scenario.

Scenario	Q (m^3/h)	Water-surface elev. (m)	Mean velocity (m/s)	Conveyance K (m^3/s)	Flow depth in the bed (m)	Regime/observation
S0 (no pumping)	0	180.15	0.00	0.00	0.15	baseline; water confined to the minor bed
S1 (low)	200	180.45	0.12	1.12	0.45	conveyance below the threshold for channelized flow; lateral stagnation
S2 (optimal)	400	180.85	0.32	2.22	0.85	minor + intermediate beds at bankfull; channelized flow
S3 (high)	600	181.25	0.41	3.33	1.25	capacity of the beds exceeded; overbank flow into the major bed

The diagnostic variables confirm the mechanism controlling the non-monotonic response. In scenario S1 the imposed discharge of 200 m^3/h is below the threshold at which the flow can be routed efficiently: the conveyance of the minor bed (1.12 m^3/s), the mean velocity (0.12 m/s) and the flow depth (0.45 m) remain low, and the corresponding water-surface elevation (180.45 m) is governed mainly by the longitudinal bed slope rather than by the discharge. The flow is therefore not confined: it spreads laterally over the flat, low-lying intermediate bed, where it stagnates in the meanders and the lowlands, which produces the largest lateral inundation (116.2 ha) among the three pumping scenarios. In scenario S2 the increase of the discharge to 400 m^3/h raises the conveyance (2.22 m^3/s) and the velocity (0.32 m/s) to values close to those of an effective channelized flow; the water

surface rises to a level close to bankfull but remains confined within the combined minor and intermediate beds, and the inundated area falls to 53 ha. Scenario S3 (600 m^3/h) exceeds the combined conveyance capacity of the two beds; the water surface rises above the bankfull level and the surplus spills into the major bed, producing 158 ha (modelled). The three scenarios thus differ not by a monotonic rise of the water level, but by the position of the water surface with respect to the bankfull threshold and by the efficiency with which the discharge is conveyed.

The field validation mission for scenario S3 confirmed the preferential flood zones identified by the model, while revealing an overestimation of 58.7% of the flooded area (58.43 ha relative to the 99.57 ha measured in the field). This overestimation can be attributed to: i) the non-consideration of flow obstacles in the major bed (culverts, embankments, dense vegetation); ii) the higher-than-expected roughness in the lowland zones occupied by crops and dense hygrophilous vegetation; and iii) the uncertainties inherent in 1D modeling that does not capture transverse flatness effects. Figures 4-7 illustrate the zones likely to be flooded during the pit dewatering for the different scenarios.

The 400 m^3/h discharge must be regarded as a conditional optimum rather than a fixed recommendation. Its validity depends i) on the pumping duration, ii) on the season and on the state of the channel, and iii) on the assumption that no rainfall occurs. A volume of 3,000,000 m^3 pumped at 400 m^3/h requires a continuous schedule of about 7500 h (≈ 312 days). Throughout this schedule the water

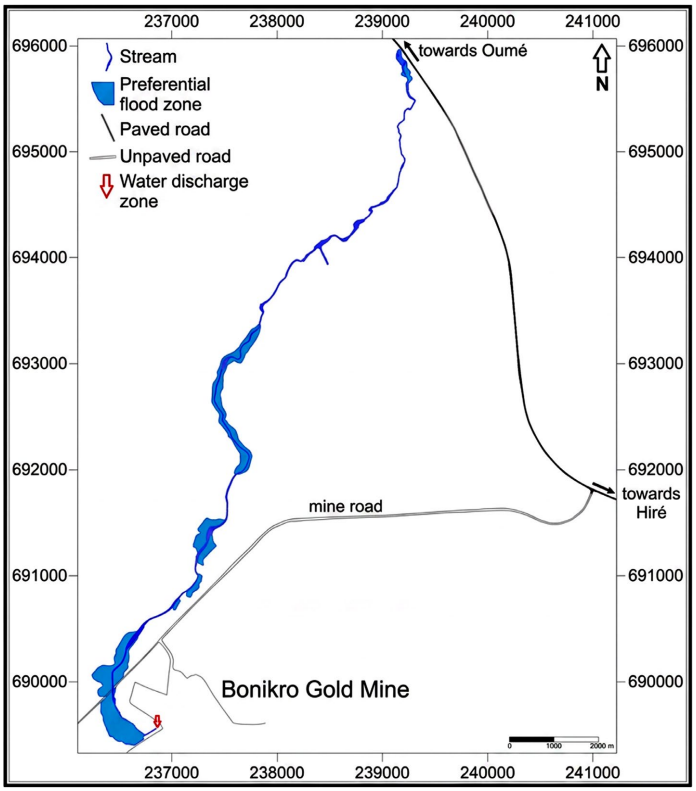


Figure 4. Modeled potential water-accumulation zones along the channel for a pumping flow of 0 m^3/h.

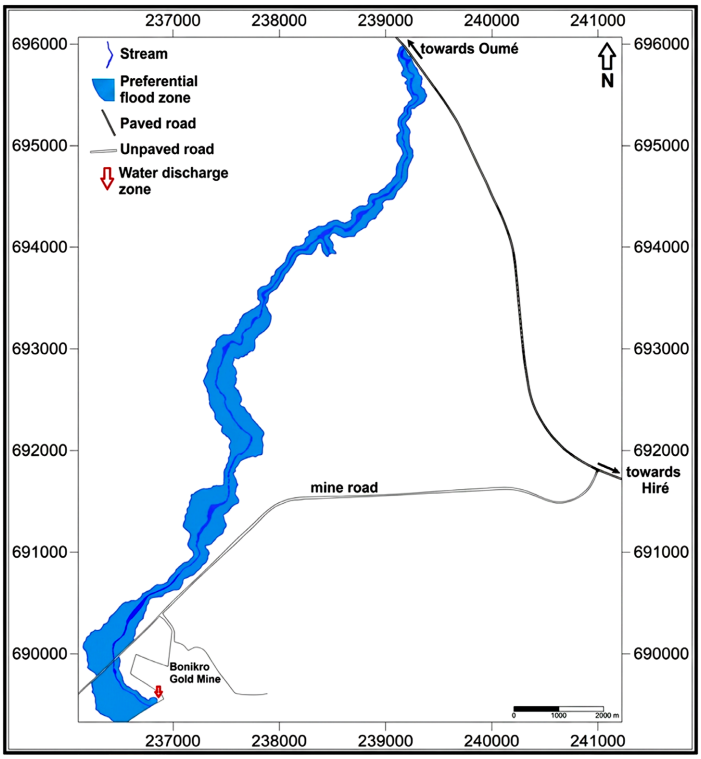


Figure 5. Modeled potential water-accumulation zones along the channel for a pumping flow of 200 m^3/h.

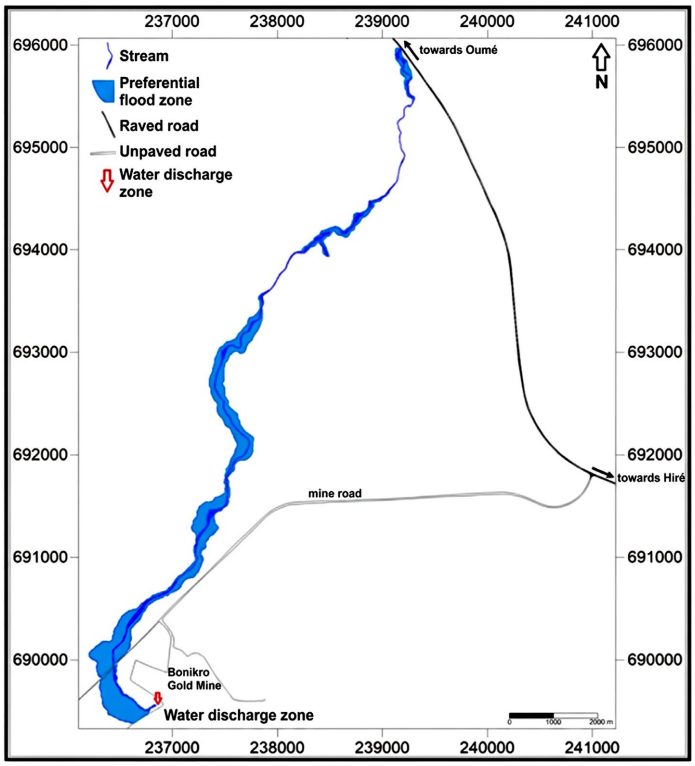


Figure 6. Modeled potential water-accumulation zones along the channel for a pumping flow of 400 m^3/h.

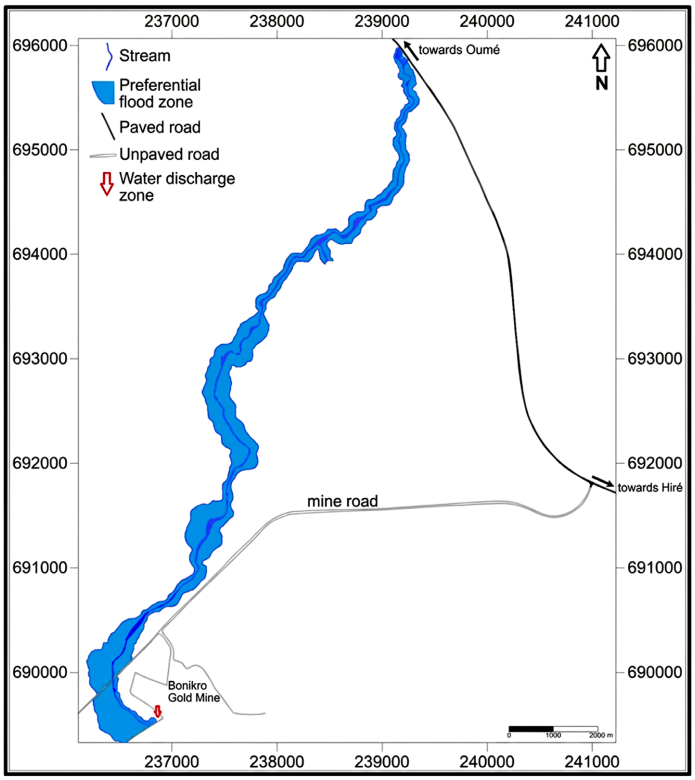


Figure 7. Modeled potential water-accumulation zones along the channel for a pumping flow of 600 m^3/h.

surface remains permanently close to the bankfull level, so that the optimum is stable only as long as the conveyance capacity of the minor and intermediate beds is maintained. Any additional natural flood, any reduction of the capacity through sedimentation or vegetation growth, or any interruption of the dredging programme would raise the water surface above bankfull and cause overbank flow into the major bed. The recommended operation is therefore a conditional window: 400 m^3/h is acceptable during the dry season and low-flow periods, whereas in the rainy season the discharge must be reduced, or the pumping temporarily suspended during flood peaks, in order to remain below the bankfull threshold.

4. Discussion

4.1. Relevance of the Methodological Approach

The combination of drone photogrammetry, terrestrial topographic surveying and HEC-RAS modeling proved particularly well adapted to the field conditions of the study area. The use of the DJI Phantom 4 RTK provided topographic data of centimeter accuracy, comparable to LiDAR surveys but at much lower cost [11] [12]. This approach is in line with the current trend of integrating UAV technologies in flood-risk studies [23] [24]. One-dimensional HEC-RAS modeling, although presenting recognized limitations [25] [26], remains a robust and accessible tool for analyzing river floods under steady conditions, particularly in contexts where available data are limited. Similar studies conducted in West Africa confirm

the relevance of this approach for delineating flood-prone areas in tropical environments [1] [27] [28].

4.2. Analysis of Flood Mechanisms

The non-monotonic relationship observed between the mine dewatering flow and the flooded area deserves in-depth hydraulic analysis. This relationship is explained by the particular morphological characteristics of the studied watercourse, notably its strong meandering character and the presence of numerous interconnected lowlands and marshes. At low flows (scenario S1, 200 m^3/h), hydraulic studies have already shown that, in highly sinuous streams, the sediment and water transport capacity is strongly reduced below a certain discharge threshold [29] [30]. Below this threshold, the flow energy is insufficient to maintain a continuous current in the channel, favoring water stagnation in the meanders and lowlands and, consequently, flooding of adjacent banks. This phenomenon is even more marked in low-gradient tropical streams [22]. At high flows (scenario S3, 600 m^3/h), flooding results from exceeding the hydraulic capacity of the channel cross-sections, a well-documented phenomenon [8]. In the present case, the existence of undersized crossing structures (culverts) constitutes a major aggravating factor, creating hydraulic blockage points that locally amplify flood levels. Similar observations have been reported by Vousdoukas *et al*. [31] and Sarhadi *et al*. [32], who underline the determining role of hydraulic structures in the dynamics of river floods.

The optimal flow of 400 m^3/h corresponds to the hydraulic capacity of the combined minor and intermediate beds. This result is consistent with the concept of dominant discharge or bankfull discharge, defined as the flow for which the watercourse exactly fills its minor bed without overflowing [33]. In tropical West African rivers, this discharge generally corresponds to a recurrence of 1.5 to 2 years [34] [35], consistent with the field observations. The results presented here are consistent with the work of Patel *et al*. [9] and Quirogaa *et al*. [26], who highlight the tendency of 1D HEC-RAS models to overestimate flooded areas in the presence of high floodplain roughness. It should be stressed that the value of 400 m^3/h identified here is a conditional optimum: it holds for the dry-season, low-flow conditions under which it was established and for a pumping schedule compatible with the conveyance capacity of the minor and intermediate beds; it cannot be extrapolated to the rainy season or to a modified channel geometry without a new simulation.

4.3. Uncertainty Analysis and Model Limitations

The 58.7% discrepancy observed between the modelled (158 ha) and field-measured (99.57 ha) flooded areas for scenario S3 raises the question of the limits of 1D hydraulic modeling in floodplain environments. Several studies have documented this limitation. Néelz and Pender [25] showed that 1D models systematically overestimate flooded areas compared with 2D models, particularly in zones

of high floodplain roughness. Quirogaa *et al*. [26] quantified this overestimation between 15 and 45% depending on the terrain characteristics, the 58.7% obtained here falling slightly above this range, which is consistent with the particularly dense floodplain vegetation and the abundance of anthropogenic obstacles in the present study area. Teng *et al*. [7], in their comprehensive review of flood modeling approaches, stress that 1D models are particularly sensitive to the quality of floodplain topographic data and to the accuracy of the roughness coefficients assigned to the different flow zones.

In the present study, the lowlands occupied by market gardens and dense hygrophilous vegetation present a roughness clearly higher than that of the main channel, which slows lateral flow and effectively reduces the flooded area compared with the model predictions. Furthermore, the non-integration of anthropogenic obstacles (track embankments, undersized culverts, agricultural dikes) in the 1D model geometry constitutes a significant source of uncertainty. These obstacles act as hydraulic barriers that fragment the floodable space into distinct compartments, reducing the hydraulic connectivity between the channel and its floodplain [6] [36]. This limitation argues for the use, in future similar studies, of two-dimensional (2D) or coupled 1D/2D hydraulic modeling, enabled by tools such as HEC-RAS 2D [8], TELEMAC-2D [37] or MIKE FLOOD [38], combined with high-resolution topographic data derived from drone photogrammetry.

4.4. Role of Hydraulic Structures in Flood Dynamics

The identification of undersized culverts as an aggravating factor of flooding deserves particular attention. These crossing structures, built to allow rural tracks to pass over the watercourse, create hydraulic constriction zones that locally induce a rise in water levels upstream and a slowing of the flow [31] [32]. This phenomenon is particularly pronounced during flood events, when the discharge exceeds the nominal capacity of these structures. In the tropical African context, the undersizing of crossing structures is a recurrent problem, often related to the lack of prior hydraulic studies in their design [28] [39]. The recommendation to replace existing culverts with better-sized structures, formulated in the present study, is part of this perspective of improving the overall hydraulic capacity of the flow system. The dredging of the flow channel, also recommended, aims to reduce the roughness of the minor bed and to remove the sedimentary and vegetal obstacles that locally reduce the available hydraulic cross-section. Studies conducted in similar contexts have shown that regular dredging of tropical channels can increase the hydraulic capacity of the minor bed by 20 to 40%, reducing accordingly the risk of overflow during floods [40].

5. Conclusion

This study assessed the hydraulic impacts of the discharge of Bonikro Gold mine pit dewatering waters on the downstream alluvial plain, through a multidiscipli-

nary approach combining RTK drone imagery, topographic surveys, hydrogeomorphological analysis and HEC-RAS hydraulic modeling. The main results can be summarized as follows: i) the morphology of the receiving watercourse is characterized by a high degree of sinuosity, with lowlands and marshes constituting potentially flood-prone zones highly sensitive to changes in hydraulic regime; ii) the discharge-flooded area relationship is non-monotonic, with a hydraulic optimum, conditional on the pumping duration and the season, corresponding to a discharge of 400 m^3/h, for which the minor and intermediate beds effectively absorb the pumped water volume, limiting the flooded area to 53 ha against 16.9 ha in the natural state; iii) the extreme scenarios of 200 m^3/h and 600 m^3/h generate clearly more extensive floods (116.2 ha and 99.57 - 158 ha respectively), through distinct hydraulic mechanisms—stagnation for the low flow, overflow for the high flow; iv) the field validation of the 600 m^3/h scenario revealed an overestimation of 58.7% by the 1D model (58.43 ha relative to the 99.57 ha measured in the field), illustrating the limits of one-dimensional modeling in a floodplain occupied by dense vegetation and anthropogenic obstacles; and v) the operational recommendations formulated (channel dredging, culvert replacement, dry-season dewatering, conditional optimal discharge of 400 m^3/h and real-time monitoring) constitute a coherent and applicable management plan for minimizing the environmental and socio-economic impacts of pit dewatering. These results contribute to the knowledge base on the hydraulic management of mine dewatering waters in humid tropical environments and illustrate the value of combining UAV technologies and HEC-RAS modeling for environmental decision support in the African mining sector.

Acknowledgements

The authors thank the management of the Bonikro Gold mine for commissioning and funding this study, as well as the technical teams who took part in the January-February 2021 field missions. Our thanks also go to the riparian farming communities for their cooperation and the valuable information provided during the field surveys.

Author Contributions

Conceptualisation, Yao, B.K. and Touré, M., Anzoumanan, K.; methodology, Yao, B.K.; Anzoumanan, K., investigation, Yao, B.K., Touré, M., and Baka, D.; data curation, Yao, B.K.; formal analysis, Yao, B.K., Touré, M., Anzoumanan, K. and Baka, D.; Validation, Yao, B.K.; Visualization, Baka, D.; writing, review and editing, Yao, B.K. and Anzoumanan, K.; supervision, Anzoumanan, K.; project administration, Yao, B.K.

All authors have read and agreed.

Conflicts of Interest

The authors declare no conflict of interest.

References

[1] Diallo, A., Doumbia, M., Mahé, G., Cissé, M.T. and Diabaté, L. (2019) Cartographie et évaluation du risque d'inondation dans le bassin versant du Niandan (Guinée). *Revue Des Sciences De L'Eau*, **32**, 227-245.

[2] Ouattara, I., Kouamé, K.F., Kouassi, A.M., Kouakou, K.E. and Biemi, J. (2021) Impact des activités minières sur la qualité des eaux de surface et souterraines dans la région du Centre de la Côte d'Ivoire. *International Journal of Biological and Chemical Sciences*, **15**, 207-224.

[3] Rakotondrabe, F., Ndam Ngoupayou, J.R., Mfonka, Z., Rasolomanana, E.H., Nyangono Abolo, A.J. and Ako Ako, A. (2018) Water Quality Assessment in the Bétaré-Oya Gold Mining Area (East-Cameroon): Multivariate Statistical Analysis Approach. *Science of the Total Environment*, **610**, 831-844. https://doi.org/10.1016/j.scitotenv.2017.08.080

[4] Plate, E.J. (2002) Flood Risk and Flood Management. *Journal of Hydrology*, **267**, 2-11. https://doi.org/10.1016/s0022-1694(02)00135-x

[5] Jonkman, S.N. and Vrijling, J.K. (2008) Loss of Life Due to Floods. *Journal of Flood Risk Management*, **1**, 43-56. https://doi.org/10.1111/j.1753-318x.2008.00006.x

[6] Dottori, F., Salamon, P., Bianchi, A., Alfieri, L., Hirpa, F.A. and Feyen, L. (2016) Development and Evaluation of a Framework for Global Flood Hazard Mapping. *Advances in Water Resources*, **94**, 87-102. https://doi.org/10.1016/j.advwatres.2016.05.002

[7] Teng, J., Jakeman, A.J., Vaze, J., Croke, B.F.W., Dutta, D. and Kim, S. (2017) Flood Inundation Modelling: A Review of Methods, Recent Advances and Uncertainty Analysis. *Environmental Modelling & Software*, **90**, 201-216. https://doi.org/10.1016/j.envsoft.2017.01.006

[8] Brunner, G.W. (2016) HEC-RAS River Analysis System Hydraulic Reference Manual, Version 5.0. US Army Corps of Engineers, Hydrologic Engineering Center, CPD-69, 538 p.

[9] Patel, D.P., Ramirez, J.A., Srivastava, P.K., Bray, M. and Han, D. (2017) Assessment of Flood Inundation Mapping of Surat City by Coupled 1D/2D Hydrodynamic Modeling: A Case Application of the New HEC-RAS 5. *Natural Hazards*, **89**, 93-130. https://doi.org/10.1007/s11069-017-2956-6

[10] Nex, F. and Remondino, F. (2014) UAV for 3D Mapping Applications: A Review. *Applied Geomatics*, **6**, 1-15. https://doi.org/10.1007/s12518-013-0120-x

[11] Benassi, F., Dall'Asta, E., Diotri, F., Forlani, G., Morra di Cella, U., Roncella, R., *et al*. (2017) Testing Accuracy and Repeatability of UAV Blocks Oriented with GNSS-Supported Aerial Triangulation. *Remote Sensing*, **9**, Article No. 172. https://doi.org/10.3390/rs9020172

[12] Tomaštík, J., Mokroš, M., Surový, P., Grznárová, A. and Merganič, J. (2019) UAV RTK/PPK Method—An Optimal Solution for Mapping Inaccessible Forested Areas? *Remote Sensing*, **11**, Article No. 721. https://doi.org/10.3390/rs11060721

[13] Schumann, G., Bates, P.D., Horritt, M.S., Matgen, P. and Pappenberger, F. (2009) Progress in Integration of Remote Sensing-Derived Flood Extent and Stage Data and Hydraulic Models. *Reviews of Geophysics*, **47**, RG4001. https://doi.org/10.1029/2008rg000274

[14] Yan, K., Di Baldassarre, G., Solomatine, D.P. and Schumann, G.J. (2015) A Review of Low-Cost Space-Borne Data for Flood Modelling: Topography, Flood Extent and Water Level. *Hydrological Processes*, **29**, 3368-3387.

https://doi.org/10.1002/hyp.10449

[15] Aristodemou, E. and Bruder, A. (2017) A Framework for the Assessment of Flood Hazard and Risk Using High-Resolution Unmanned Aerial Vehicle (UAV) Imagery. *Natural Hazards*, **88**, 1205-1225.

[16] Lucieer, A., Jong, S.M.d. and Turner, D. (2014) Mapping Landslide Displacements Using Structure from Motion (SfM) and Image Correlation of Multi-Temporal UAV Photography. *Progress in Physical Geography*: *Earth and Environment*, **38**, 97-116. https://doi.org/10.1177/0309133313515293

[17] US Army Corps of Engineers (USACE) (2016) HEC-RAS River Analysis System, 2D Modeling User's Manual, Version 5.0. Hydrologic Engineering Center.

[18] Gravelius, H. (1914) Grundriss der gesamten Gewässerkunde, Band I: Flusskunde. Göschen, 265 p.

[19] Bendjoudi, H. and Hubert, P. (2002) Le coefficient de compacité de Gravelius: Analyse critique d'un indice de forme des bassins versants. *Hydrological Sciences Journal*, **47**, 921-930. https://doi.org/10.1080/02626660209493000

[20] Musy, A. (2001) Hydrologie générale. Presses Polytechniques et Universitaires Romandes (PPUR), 312 p.

[21] Roche, M. (1963) Hydrologie de surface. Gauthier-Villars, 352 p.

[22] Huang, H.Q., Nanson, G.C. and Fagan, S.D. (2002) Hydraulic Geometry of Straight Alluvial Channels and the Principle of Least Action. *Journal of Hydraulic Research*, **40**, 153-160. https://doi.org/10.1080/00221680209499858

[23] Langhammer, J., Vacková, T. and Guth, J. (2017) Unstructured Grid Model for Flood-Plain Inundation in Heterogeneous Landscapes Using UAV Photogrammetry. *Remote Sensing*, **9**, Article No. 672.

[24] Mišijovský, J. and Langhammer, J. (2015) Multitemporal Monitoring of the Morphodynamics of a Mid-Mountain Stream Using UAS Photogrammetry. *Remote Sensing*, **7**, 8586-8609. https://doi.org/10.3390/rs70708586

[25] Néelz, S. and Pender, G. (2013) Benchmarking the Latest Generation of 2D Hydraulic Modelling Packages. Environment Agency, Report SC120002, 189 p.

[26] Quirogaa, V.M., Kurea, S., Udoa, K. and Manoa, A. (2016) Application of 2D Numerical Simulation for the Analysis of the February 2014 Bolivian Amazonia Flood: Application of the New HEC-RAS Version 5. *Ribagua*, **3**, 25-33. https://doi.org/10.1016/j.riba.2015.12.001

[27] Zannou, A., Hounkpè, J., Diekkrüger, B. and Afouda, A. (2011) Estimation des débits extrêmes dans les bassins versants non jaugés: Application au bassin versant de l'Ouémé à Bétérou (Bénin). *Revue Des Sciences De L'Eau*, **24**, 241-254.

[28] Konaté, I., Kouassi, A.M., Koffi, K., Kouamé, K.F. and Biemi, J. (2018) Analyse hydrogéomorphologique pour la cartographie des zones inondables dans le bassin versant de la Lobo (Centre-Ouest, Côte d'Ivoire). *Revue Des Sciences De L'Eau*, **31**, 141-158.

[29] Leopold, L.B. and Wolman, M.G. (1960) River Meanders. *Geological Society of America Bulletin*, **71**, 769-794. https://doi.org/10.1130/0016-7606(1960)71[769:rm]2.0.co;2

[30] Schumm, S.A. (1977) The Fluvial System. John Wiley & Sons, 338 p.

[31] Vousdoukas, M.I., Mentaschi, L., Voukouvalas, E., Verlaan, M., Jevrejeva, S., Jackson, L.P., *et al*. (2018) Global Probabilistic Projections of Extreme Sea Levels Show Intensification of Coastal Flood Hazard. *Nature Communications*, **9**, Article No. 2360.

https://doi.org/10.1038/s41467-018-04692-w

[32] Sarhadi, A., Soltani, S. and Modarres, R. (2012) Probabilistic Flood Inundation Mapping of Ungauged Rivers: Linking GIS Techniques and Frequency Analysis. *Journal of Hydrology*, **458**, 68-86. https://doi.org/10.1016/j.jhydrol.2012.06.039

[33] Williams, G.P. (1978) Bank-Full Discharge of Rivers. *Water Resources Research*, **14**, 1141-1154. https://doi.org/10.1029/wr014i006p01141

[34] Ouédraogo, W.A.A., Garambe, T.E., Gado Djibo, A. and Paturel, J.E. (2016) Analyse fréquentielle des crues des cours d'eau du Burkina Faso. *Revue Des Sciences De L'Eau*, **29**, 105-122.

[35] Cissé, M.T., Mahé, G., Paturel, J.E., Diallo, A. and Moussa, I.B. (2018) Caractérisation des débits de crues et des étiages des cours d'eau de Guinée (Afrique de l'Ouest). *Revue Des Sciences De L'Eau*, **31**, 15-32.

[36] Vogt, J.V., Soille, P., de Jager, A., Rimaviciute, E., Mehl, W., Foisneau, S., Bódis, K., Dusart, J., Paracchini, M.L., Haastrup, P. and Bamps, C. (2011) A Pan-European River and Catchment Database. Report EUR 22920 EN, European Commission, 120 p.

[37] Hervouet, J.M. (2007) Hydrodynamics of Free Surface Flows: Modelling with the Finite Element Method. Wiley, 341 p. https://doi.org/10.1002/9780470319628

[38] DHI (2017) MIKE FLOOD User Manual. DHI Water and Environment, 156 p.

[39] Sangare, S., Coulibaly, Y., Cissé, G., Boelee, E. and Wyss, K. (2020) Gouvernance de l'eau en zones rurales de l'Afrique de l'Ouest: Enjeux hydrauliques et défis institutionnels. *Cahiers Agricultures*, **29**, 7.

[40] Traore, V.B., Sambou, S., Sambou, H., Tamba, S., Diaw, A.T. and Coly, A. (2019) Modélisation hydraulique des crues du fleuve Casamance à Kolda (Sénégal). *Revue Des Sciences De L'Eau*, **32**, 53-68.